Maximum likelihood estimators and Cramér–Rao bound for estimating azimuth and elevation angles using compact arrays

Ildar R. Urazghildiiev[1,a)] and David Hannay[2]
[1]*JASCO Applied Sciences (Alaska) Inc., Anchorage, Alaska 99501, USA*
[2]*JASCO Applied Sciences (Canada) Ltd., Victoria, Canada*

(Received 12 December 2016; revised 20 March 2017; accepted 23 March 2017; published online 11 April 2017)

The problem of estimating the azimuth and elevation angle of a sound source using a compact array of hydrophones is addressed. The closed-form representations for several time-difference of arrival (TDOA) based estimators are given, and their accuracies are evaluated using both statistical simulations and *in situ* tests. Simulations demonstrated that the accuracy provided by the estimators is close to the Cramér–Rao bounds. In real conditions, the main cause of azimuth and elevation errors can be refraction, surface and bottom reflections and other unpredictable sound propagation effects resulting in large and slowly changing errors. © *2017 Acoustical Society of America*.
[http://dx.doi.org/10.1121/1.4979792]

[JFL] Pages: 2548–2555

I. INTRODUCTION

Compact arrays of hydrophones provide an important ability to solve the problem of estimating azimuth and elevation angles of detected sounds[1–15] (hereafter, we refer to this problem as direction finding). This ability makes compact arrays an extremely efficient tool to detect and track marine mammals[2–9] and vessels.[10–15] Direction finding algorithms used in compact arrays are based on estimating the time-difference of arrival (TDOA) for the same signal detected on multiple hydrophones. Despite growing theoretical and practical interest in compact arrays, a number of important issues have not been addressed in the published literature.

In the majority of publications, the chosen direction finding algorithm is insufficiently supported. A technique used in many systems is a search-free (SF) estimator based on a far field approximation of TDOA.[2–8,10,11] However, this approach has no statistical motivation and is not statistically optimal. The main alternative to this algorithm is the maximum likelihood (ML) approach,[8,16–18] which should also be tested as a possible solution for use in compact arrays.

Furthermore, the potential accuracy of direction finders based on using phase differences between signals is well studied in the literature,[1,13–15,18] but there is little information about the accuracy of azimuth and elevation estimates provided by the TDOA-based estimators. The lowest variance that a TDOA-based linear estimator can achieve is specified by the Cramér–Rao bounds[17–19] (CRB). However, the closed form representations for CRB of azimuth and elevation estimates provided by TDOA-based compact arrays are unknown from the literature. It is evident that the accuracy of azimuth and elevation estimates can differ depending on algorithm design features, signal features, background noise conditions, and other factors. Estimation accuracy is not readily predictable. Taking these considerations into account, an analysis of the performance of direction finding algorithms as applied to compact arrays is an important practical problem.

In this paper, we address the problem of TDOA-based estimation of azimuth and elevation angles of underwater sound sources using compact volumetric arrays of hydrophones. Although we only address this problem for the underwater context, these evaluations are applicable to in-air microphone arrays.[20–22] The goals of this work are to provide the closed-form representations for the ML and generalized SF algorithms, to derive the closed-form representations for the CRB, and to evaluate the performance of the TDOA-based direction finders using statistical simulations and *in situ* tests. The main contribution of this paper comes from the results of a comparative analysis of the estimation accuracy from the algorithms under various conditions.

This paper is organized as follows. In Sec. II, the data model is considered, and the problem is formulated. The closed-form representations of the estimators are given in Sec. III. The Cramér–Rao bounds are derived in Sec. IV. The results of comparative analysis are considered in Sec. V. The discussion is presented in Sec. VI. Section VII provides the conclusions.

II. DATA MODEL AND PROBLEM FORMULATION

This study assumes that sources are localized within an area specified in a three-dimensional (3D) Cartesian coordinate system with the origin, O, located at the depth, z_0, relative to the sea surface. Axis OX and OY are placed in a horizontal surface, axis OY is directed to true North, and axis OZ is directed upright. The sound source is located at an unknown position specified by the vector

[a)]Electronic mail: ildar.urazghildiiev@jasco.com

 0001-4966/2017/141(4)/2548/8/$30.00 © 2017 Acoustical Society of America

$$\boldsymbol{r}(\boldsymbol{\theta}) = \begin{bmatrix} x \\ y \\ z \end{bmatrix} = r \begin{bmatrix} \cos\beta \sin\alpha \\ \cos\beta \cos\alpha \\ \sin\beta \end{bmatrix} \in \mathcal{R}^3, \quad (1)$$

where

$$\boldsymbol{\theta} = [\alpha,\ \beta,\ r]^T \quad (2)$$

is the vector of unknown parameters of a source; symbol $|\cdot|$ denotes the vector norm; x, y, and z are rectangular coordinates of the source; $r = |\boldsymbol{r}|$ is the source range; α and β are azimuth and elevation angle, respectively; and the superscript $^{\mathrm{T}}$ denotes transposed. Azimuth is measured relative to true North (axis OY) and elevation is measured relative to the horizontal plane.

The signal emitted by the source is assumed to be a random process with non-uniform power spectrum density, such that most signal energy is concentrated within the frequency band $B_S = [F_{\min}, F_{\max}]$. The sensors (hydrophones) provide low-pass filtering and synchronized digitizing of the continuous-time acoustic field with the sampling rate $F_S > 2F_{\max}$.

It is assumed that the compact array consists of $N \geq 3$ omnidirectional sensors located at known positions. Sensor positions are specified by the vectors $\boldsymbol{r}_i \in \mathcal{R}^3$, $i = 1, 2, \ldots, N$. We also assume that the source is located in far field, such that the maximum distance between sensors is much shorter than the minimum sensor-to-source distance,

$$\max_{i,j}\{|\boldsymbol{r}_i - \boldsymbol{r}_j|\} \ll \min_{i}\{|\boldsymbol{r}_i - \boldsymbol{r}|\}, \quad i,j = 1, 2, \ldots, N. \quad (3)$$

The signal propagation delay observed at the ith sensor is

$$\tau_i = \tau_i(\boldsymbol{\theta}) = |\boldsymbol{r}(\boldsymbol{\theta}) - \boldsymbol{r}_i|/c, \quad (4)$$

where c is the speed of sound. We assume a relatively uniform sound velocity profile such that sound propagation effects are not taken into consideration. Such an assumption simplifies the algorithm design and is acceptable within the small dimensions of the array, but it could cause additional estimation errors if a source was far away from an array. The TDOA between the signal replicas observed at different sensors is denoted by

$$\tau_{i,j}(\boldsymbol{\theta}) = \tau_j - \tau_i = (|\boldsymbol{r}(\boldsymbol{\theta}) - \boldsymbol{r}_j| - |\boldsymbol{r}(\boldsymbol{\theta}) - \boldsymbol{r}_i|)/c, \quad i < j. \quad (5)$$

TDOA is an unknown parameter and should be estimated from the sensor outputs. Denote the matrix of the true TDOAs by $\boldsymbol{T} = \{\tau_{i,j}(\boldsymbol{\theta}),\ i,j = 1, \ldots, N\}$.

For each time instance, t, when the presence of signal is detected, the TDOA estimates can be computed from the waveform cross-correlation function[17]

$$\rho_{i,j}(t,\tau) = \sum_n u_i(t+n)u_j(t+n+\tau) \quad (6)$$

as

$$\hat{\tau}_{i,j} = arg\max_{\tau} \rho_{i,j}(t,\tau) = \tau_{i,j}(\boldsymbol{\theta}) + \varepsilon_{i,j}, \quad (7)$$

where $u_i(t)$ is the filtered process on the output of the ith sensor; $\varepsilon_{i,j}$ is the TDOA estimation error; and symbol "^" denotes the estimate.

Let $\hat{\boldsymbol{T}} = \{\hat{\tau}_{i,j},\ i,j = 1, \ldots, N\}$ denote a matrix of TDOA estimates. We assume that a total of $N(N-1)/2$ independent measurements of signal TDOAs are performed, such that $\hat{\tau}_{i,j} = -\hat{\tau}_{j,i}$. It is also assumed that TDOA estimation errors are independent, identically distributed (i.i.d.) Gaussian variables with zero mean and covariance matrix $\sigma^2\boldsymbol{I}$, such that the TDOA estimates $\hat{\tau}_{i,j}$ are also Gaussian variables with the mean $E\{\hat{\tau}_{i,j}\} = \tau_{i,j}(\boldsymbol{\theta})$ and the variance σ^2. The assumption of i.i.d. Gaussian errors significantly simplifies the estimator design and seems to be realistic for compact arrays. However, other models, such as Gaussian variables with a non-diagonal covariance matrix, could be used, if needed. The probability density function of the TDOA estimates (7) is

$$W(\hat{\boldsymbol{T}}|\boldsymbol{\theta}) = k\exp\left\{-\frac{1}{2\sigma^2}\sum_i\sum_j\left(\hat{\tau}_{i,j} - \tau_{i,j}(\boldsymbol{\theta})\right)^2\right\}, \quad i<j, \quad (8)$$

where k is a scalar, which is independent of the signal parameters.

The problem considered in this paper can be formulated as follows: derive the closed-form representations for the practical estimators of the unknown parameters (1), $\hat{\boldsymbol{\theta}} = \hat{\boldsymbol{\theta}}(\hat{\boldsymbol{T}})$, and evaluate their accuracy using Cramér–Rao bounds, statistical simulations, and *in situ* measurements.

III. DIRECTION FINDING USING COMPACT ARRAYS

For the Gaussian distributed TDOA measurements (7), a ML estimator is optimal in that it provides accuracy close to the CRB representing the lower bound of the parameter estimation error.[18,19] Although the optimality of the ML estimator does not necessarily mean that this is the best estimator to use or even that is a satisfactory estimator, it is necessary to compare the accuracy provided by the practical estimators with those that can be obtained using the optimal ML technique.

A. Maximum likelihood estimators

If a variance of TDOA estimation error is equal for all channel pairs, the structure of the ML estimator is independent of the parameter σ^2, and the ML estimates of vector $\boldsymbol{\theta}$ can be represented as

$$\hat{\boldsymbol{\theta}}_{ML}(\hat{\boldsymbol{T}}) = arg\min_{\boldsymbol{\theta}} \sum_i\sum_j (\hat{\tau}_{i,j} - \tau_{i,j}(\boldsymbol{\theta}))^2, \quad i<j. \quad (9)$$

Nonlinear optimization problem (9) has no analytical solution and the parameters α, β, r must be searched in 3D space to compute the estimates (9). As it was shown in Ref. 17, TDOA-based direction finding algorithms are unsuitable for accurately estimating ranges, r, if the source is far from the array. Since for compact arrays the condition (3) always holds, the direction finding problem is reduced to finding

azimuth and elevation estimates, such that a practical ML estimator should only evaluate parameters α and β. The ML estimates of the azimuth and elevation angle can be obtained from (9) by using some scalar r_0 that satisfies the condition $r_0 \gg \max_{i,j}\{|\boldsymbol{r}_i - \boldsymbol{r}_j|\}$ instead of an unknown range. Then the 2D ML estimator is

$$\{\hat{\alpha}, \hat{\beta}\} = arg \min_{\alpha,\beta} \sum_i \sum_j (\hat{\tau}_{i,j} - \tau_{i,j}(\alpha, \beta, r_0))^2, \quad i < j. \tag{10}$$

The estimates (10) could be found using a 2D grid search algorithm, which is computationally expensive. However, in some cases minimizing the 2D function (10) can be replaced by minimizing two 1D functions.

Let us consider a direction finding problem in a 2D space by discarding the Z coordinate of vectors $\boldsymbol{r}$ and $\boldsymbol{r}_i$, $i = 1, 2, \ldots, N$, and assume that $\boldsymbol{r} \in \mathcal{R}^2$ and $\boldsymbol{r}_i \in \mathcal{R}^2$. If the source-to-sensor distance in the plane XOY is long enough that the condition (3) holds in the 2D space, the TDOA-based estimation of azimuth is independent of the elevation angle. Then the ML estimates of azimuth and elevation angle can be found separately. First, the azimuth estimate is computed for the certain values of range r_0 and elevation β_0:

$$\hat{\alpha} = arg \min_{\alpha} \sum_i \sum_j (\hat{\tau}_{i,j} - \tau_{i,j}(\alpha, \beta_0, r_0))^2. \tag{11a}$$

In practice, the scalar β_0 can be equal zero, $\beta_0 = 0$. Then the elevation estimate is evaluated for the azimuth estimate (11a):

$$\hat{\beta} = arg \min_{\beta} \sum_i \sum_j (\hat{\tau}_{i,j} - \tau_{i,j}(\hat{\alpha}, \beta, r_0))^2. \tag{11b}$$

Note that the estimator (11) is computationally more efficient as compared to the estimator (10) since it can be implemented by using 1D grid search. Further computational efficiency can be achieved by using the search-free estimators.

B. Search-free estimator

If the condition (3) holds, the TDOA (5) can be approximated as

$$\tau_{i,j}(\boldsymbol{\theta}) = \tau_j - \tau_i \approx -\left(\boldsymbol{r}_j^T \boldsymbol{e}(\boldsymbol{\theta}) - \boldsymbol{r}_i^T \boldsymbol{e}(\boldsymbol{\theta})\right) \Big/ c = -\frac{1}{c} \boldsymbol{d}_{i,j}^T \boldsymbol{e}(\boldsymbol{\theta}), \tag{12}$$

where

$$\boldsymbol{e}(\boldsymbol{\theta}) = \boldsymbol{r}(\boldsymbol{\theta}) / |\boldsymbol{r}(\boldsymbol{\theta})| = \begin{bmatrix} e_x \\ e_y \\ e_z \end{bmatrix} = \begin{bmatrix} \cos\beta \sin\alpha \\ \cos\beta \cos\alpha \\ \sin\beta \end{bmatrix} \in \mathcal{R}^3 \tag{13}$$

is the unit vector specifying the direction to the source, and $\boldsymbol{d}_{i,j} = \boldsymbol{r}_j - \boldsymbol{r}_i$. Approximation (12) in the matrix form can be represented as

$$\boldsymbol{\tau}(\boldsymbol{\theta}) = -\frac{1}{c} \boldsymbol{D} \boldsymbol{e}(\boldsymbol{\theta}), \tag{14}$$

where $\boldsymbol{\tau}(\boldsymbol{\theta}) = [\tau_{1,2}(\boldsymbol{\theta}), \tau_{1,3}(\boldsymbol{\theta}), \ldots, \tau_{N-1,N}(\boldsymbol{\theta})]^T \in \mathcal{R}^{N(N-1)/2}$ is the vector consisting of all $N(N-1)/2$ TDOAs (5) and $\boldsymbol{D} = [\boldsymbol{d}_{1,2}^T, \boldsymbol{d}_{1,3}^T, \ldots, \boldsymbol{d}_{N-1,N}^T]^T \in \mathcal{R}^{N(N-1)/2 \times 3}$ is the matrix composed of the vectors $\boldsymbol{d}_{i,j}$. From (14) it follows

$$\boldsymbol{e}(\boldsymbol{\theta}) = -\frac{1}{c} (\boldsymbol{D}^T \boldsymbol{D})^{-1} \boldsymbol{D}^T \boldsymbol{\tau}(\boldsymbol{\theta}). \tag{15}$$

Substituting the TDOA estimates (7) instead of unknown true TDOAs in (15), we can obtain the estimate of the directional vector:

$$\hat{\boldsymbol{e}} = -\frac{1}{c} (\boldsymbol{D}^T \boldsymbol{D})^{-1} \boldsymbol{D}^T \hat{\boldsymbol{\tau}}, \tag{16}$$

where $\hat{\boldsymbol{\tau}} = [\hat{\tau}_{1,2}, \hat{\tau}_{1,3}, \ldots, \hat{\tau}_{N-1,N}]^T \in \mathcal{R}^{N(N-1)/2}$. Then the search-free (SF) estimates of the azimuth and the elevation angle can be found from (16) as

$$\hat{\alpha} = \tan^{-1} \frac{\hat{e}_x}{\hat{e}_y} \tag{17a}$$

$$\hat{\beta} = \cos^{-1} \hat{e}_z = \tan^{-1} \frac{\hat{e}_z}{\sqrt{\hat{e}_x^2 + \hat{e}_y^2}}. \tag{17b}$$

Note that a similar estimator using a reduced number of $N-1$ TDOA estimates was used in Refs. 2–7, 10, and 11. The algorithm (17) represented here can be considered as a generalized SF estimator based of the far field approximation of TDOAs.

IV. CRAMÉR–RAO BOUND

The CRB is the lowest variance that an unbiased linear estimator can achieve. It is derived to be[18,19]

$$\mathrm{CRB}(\boldsymbol{\theta}) = \boldsymbol{F}^{-1} \tag{18}$$

where

$$\boldsymbol{F} = E\left[\left(\frac{\partial ln W(\boldsymbol{T}|\boldsymbol{\theta})}{\partial \boldsymbol{\theta}}\right)^T \left(\frac{\partial ln W(\boldsymbol{T}|\boldsymbol{\theta})}{\partial \boldsymbol{\theta}}\right)\right] = -E\left[\frac{\partial^2 ln W(\boldsymbol{T}|\boldsymbol{\theta})}{\partial \boldsymbol{\theta} \partial \boldsymbol{\theta}^T}\right] \tag{19}$$

is the Fisher information matrix (FIM). Performing statistical averaging of the likelihood function (8), the FIM elements of can be represented as

$$(\boldsymbol{F})_{m,n} = \frac{1}{\sigma^2} \sum_i \sum_j \frac{\partial \tau_{i,j}(\boldsymbol{\theta})}{\partial \theta_m} \frac{\partial \tau_{i,j}(\boldsymbol{\theta})}{\partial \theta_n}, \quad m, n = 1 \ldots 3. \tag{20}$$

Here θ_m is the mth element of the vector $\boldsymbol{\theta}$ (2) and $(\boldsymbol{F})_{m,n}$ is the (m,n) th element of FIM (19). Partial derivative of the TDOAs (5) over the parameter θ_m is

$$\frac{\partial \tau_{i,j}(\boldsymbol{\theta})}{\partial \theta_m} = \frac{\partial t_j}{\partial \theta_m} - \frac{\partial t_i}{\partial \theta_m}. \tag{21}$$

Substituting the parameters α, β, and r in (21), we obtain representations for the partial derivatives in the closed form:

$$\frac{\partial t_i}{\partial \alpha} = \frac{1}{cd_i}\left[(x - x_i)r\cos\alpha\cos\beta - (y - y_i)r\sin\alpha\cos\beta\right], \tag{22a}$$

$$\frac{\partial t_i}{\partial \beta} = \frac{1}{cd_i}\left[-(x - x_i)r\sin\alpha\sin\beta - (y - y_i)r\cos\alpha\sin\beta + (z - z_i)r\cos\beta\right], \tag{22b}$$

$$\frac{\partial t_i}{\partial r} = \frac{1}{cd_i}\left[(x - x_i)\sin\alpha\cos\beta + (y - y_i)\cos\alpha\cos\beta + (z - z_i)\sin\beta\right], \tag{22c}$$

where $d_i = |\boldsymbol{r}(\boldsymbol{\theta}) - \boldsymbol{r}_i|$.

From Eqs. (18)–(22), the approximations of Cramér–Rao lower bounds of variances of the estimates $\hat{\alpha}$, $\hat{\beta}$, and $\hat{r}$ can be represented as follows:

$$\sigma_\alpha^2 = E\left\{(\hat{\alpha} - \alpha(\boldsymbol{\theta}))^2\right\} \geq \frac{1}{(\boldsymbol{F})_{1,1}}, \tag{23a}$$

$$\sigma_\beta^2 = E\left\{(\hat{\beta} - \beta(\boldsymbol{\theta}))^2\right\} \geq \frac{1}{(\boldsymbol{F})_{2,2}}, \tag{23b}$$

$$\sigma_r^2 = E\left\{(\hat{r} - r(\boldsymbol{\theta}))^2\right\} \geq \frac{1}{(\boldsymbol{F})_{3,3}}. \tag{23c}$$

As mentioned above, compact arrays for which the condition (3) holds are unsuitable for estimating ranges. Therefore, only variances of the estimates $\hat{\alpha}$ and $\hat{\beta}$ make practical sense and are tested in Sec. V.

V. TEST RESULTS

In this study, a tetrahedral array of underwater Autonomous Multichannel Acoustic Recorders[12] (AMARs, JASCO Applied Sciences) was used for statistical simulations and *in situ* tests. The array was deployed on the VENUS cabled ocean observatory operated by Ocean Network Canada in the Salish Sea, near Vancouver, BC, Canada. Each AMAR had four hydrophones sampling at 64 kHz using a four channel ADC to ensure simultaneous sampling. The hydrophone sensitivity and current-to-voltage converter board were −165 dB re 1 V/μPa at 250 Hz. The array was deployed at the ocean bottom at a 168 m depth, and the positions of sensors in the array were $\boldsymbol{r}_1 = [0, 0, 1.5]^T$, $\boldsymbol{r}_2 = [-0.66, -0.84, 0]^T$, $\boldsymbol{r}_3 = [1.05, -0.14, 0]^T$, and $\boldsymbol{r}_4 = [-0.41, 0.98, 0]^T$ m. The array position and orientation were measured during the deployment and calibrated using surface vessels with known GPS coordinates.

A. Statistical simulations

Two simulation scenarios were considered. In the first scenario, the empirical root-mean square error (RMSE) as a function of the source range, r, was evaluated. Without loss of generality, we simulated a source traveling from the sensor with a constant speed and the heading angle, such that the source positions were simulated as $\boldsymbol{r}(t) = \boldsymbol{r}(t_0) + V\boldsymbol{e}(\gamma)(t - t_0)$, where $\boldsymbol{r}(t_0) = [10, 10, 159]^T$ is the initial position; $V = 7$ m/s $= 13.73$ knots is the source speed; $\gamma = 45°$ is the heading angle; and $\boldsymbol{e}(\gamma) = [\sin\gamma, \cos\gamma, 0]^T$ is a unit vector describing the travel direction. Figure 1(a) shows the source range as a function of time, and Fig. 1(b) shows the azimuth and elevation angles as a function of range. In these figures, 11 simulated source positions are displayed by the circles.

For each of the simulated source positions, the azimuth and elevation estimates were computed using $L = 1000$ runs. In each run, an i.i.d. Gaussian zero-mean TDOA estimation error $\varepsilon_{i,j}$ with a standard deviation $\sigma = 10\,\mu s$ was added to the true TDOA.

Estimation accuracies provided by the ML estimators (10), (11) and the search-free algorithm (17) were tested. The empirical RMSE of the estimates $\hat{\alpha}$ and $\hat{\beta}$ were computed as

$$\mathrm{RMSE}_\theta = \sqrt{(L)^{-1}\sum_{l=1}^{L}(\hat{\theta}(l) - \theta)^2}, \quad \theta \in \{\alpha, \beta\}, \tag{24}$$

where L ($L = 1000$) is the number of simulations. For simplicity, hereafter we use the variable "θ" to define both azimuths and elevations, i.e., $\theta = \alpha$ for azimuths and $\theta = \beta$ for elevations.

Note that for unbiased estimates, the RMSE (24) is equal to the standard deviation (STD) of azimuth and elevation estimates, $\mathrm{STD}_\theta = \mathrm{RMSE}_\theta$, $\theta \in \{\alpha, \beta\}$.

In all simulations, the ML estimators (10) and (11) provided undistinguishable RMSE, such that the results displayed in this section are applicable to both 2D and 1D ML

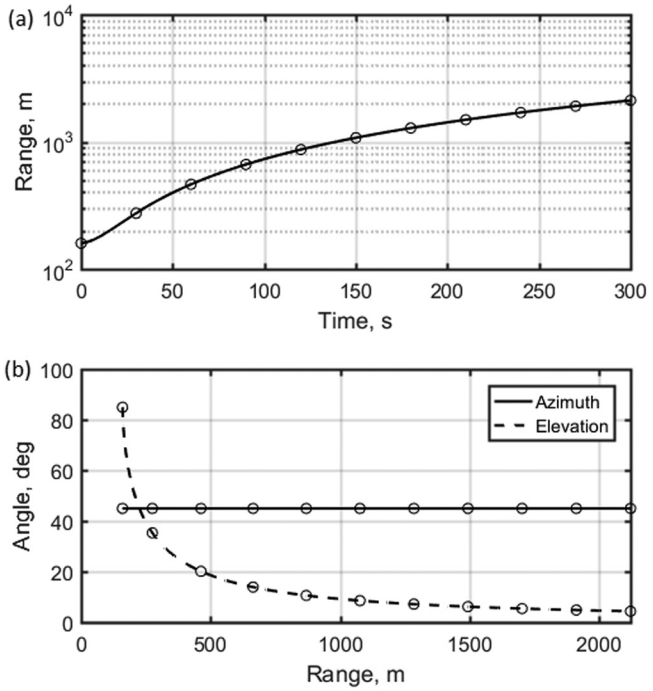

FIG. 1. (a) Source range as a function of time, (b) source azimuth and elevation angles as a function of range. Simulated source positions are displayed by the symbol "o".

estimators (10), (11). Figure 2 shows the empirical RMSE (24) of the ML estimates (10), (11), SF estimates (17), and the CRB (23) as functions of the source range.

In the second scenario, the empirical RMSE as a function of the standard deviation of TDOA estimates, σ, was evaluated. The coordinates of the source were $\boldsymbol{r} = [550,\ 350,\ 159]^T$. Figure 3 shows the CRB (23) and the empirical RMSE (24) computed for the ML estimators (10), (11) and for the SF algorithm (17).

B. *In situ* test

Data collected in the Salish Sea, near Vancouver, BC on February 21–22 and August 17–23, 2016 were used for *in situ* testing. The estimator accuracy was tested using sounds produced by 558 vessels with known GPS coordinates. We refer to these sounds as ship noise. The azimuth and elevation angles were measured using a matrix of TDOA estimates of ship noise, $\hat{\boldsymbol{T}}$, computed every 0.5 s using data segments 1 s long each and within the frequency range 50–25 000 Hz. The performance of the ML estimators (10), (11) and the SF location algorithm (17) were tested.

In all tests, the estimators (10), (11), and (17) provided basically undistinguishable results. Since the SF estimate (17) is unrestricted, the SF algorithm provided a small number of outliers in both azimuth and elevation estimates. However, the number of outliers was negligibly small, such that the results obtained for the 1D ML estimator (11) are displayed further.

An example of the ML azimuth and elevation estimates computed using the compact array are shown in Figs. 4(a) and 4(c), respectively. The dashed lines in Figs. 4(a) and 4(c) show the GPS-based azimuths and elevations of four vessels traveling near the compact array. Since the position of the GPS receiver can differ from the position of the ship engine, the GPS coordinates provided by the AIS system were adjusted to minimize the mean square error of the azimuth and elevation estimation errors. The GPS coordinates were also interpolated using the time samples to coordinate with the azimuth and elevation estimates. Figures 4(b) and 4(d) show the azimuth and elevation estimation errors, $\delta_\alpha = \alpha(\boldsymbol{r}) - \hat{\alpha}$ and $\delta_\beta = \beta(\boldsymbol{r}) - \hat{\beta}$. Here $\alpha(\boldsymbol{r})$ and $\beta(\boldsymbol{r})$ are the azimuth and elevations of a vessel located at the point $\boldsymbol{r}$. The x and y coordinates (1) of the vector $\boldsymbol{r}$ were computed using the GPS coordinates of a vessel, and the z coordinate was assumed $z = 158$ m for all vessels. Figure 5 shows the GPS-based ranges of the four vessels.

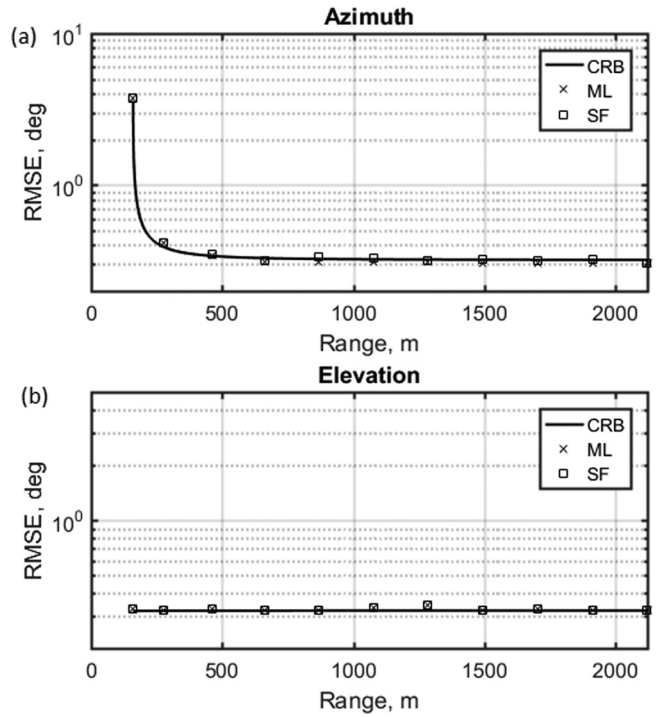

FIG. 2. CRB and empirical RMSE as a function of the source range, r, computed for the ML estimators and for the SF algorithm.

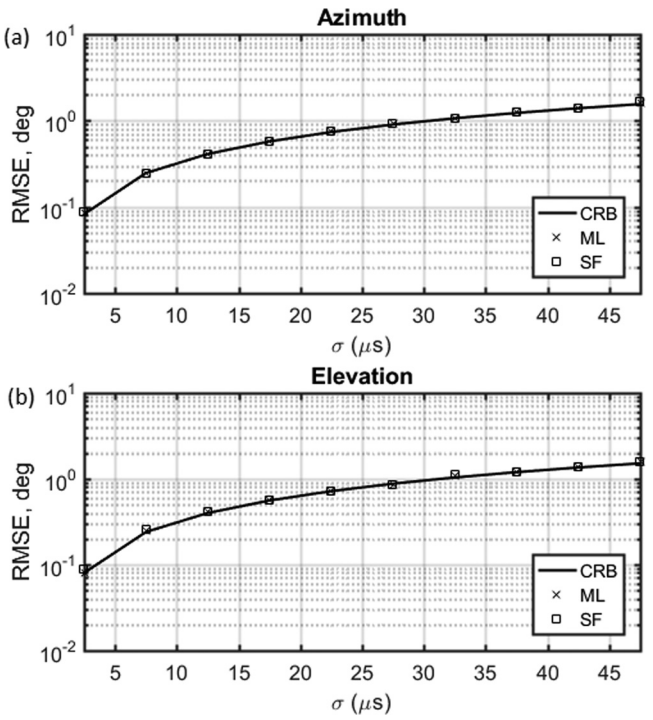

FIG. 3. CRB and empirical RMSE as a function of the standard deviation of TDOA estimates, σ, computed for the ML estimators and for the SF algorithm.

Figures 4(b) and 4(d) indicate that azimuth and elevation errors can be represented as an additive sum of two components. The first component represents relatively large and slowly changing errors with the correlation interval longer than 1 min. The second component corresponds to small almost uncorrelated errors occurring around large errors. On the basis of this observation, we represented azimuth and elevation errors as follows:

$$\delta_\theta = \hat{\theta} - \theta(\boldsymbol{r}) = b_\theta + \varepsilon_\theta, \quad \theta \in \{\alpha, \beta\}, \tag{25}$$

where $\theta = \alpha$ for the azimuths and $\theta = \beta$ for the elevations, respectively; b_θ is a large and slowly changing error, and ε_θ is a small uncorrelated error that can be modeled as an i.i.d. Gaussian random variable. Local variations of azimuth and elevation estimates are much smaller than their slowly changing deviations, such that their statistical properties are expected to be different, in particular the variances

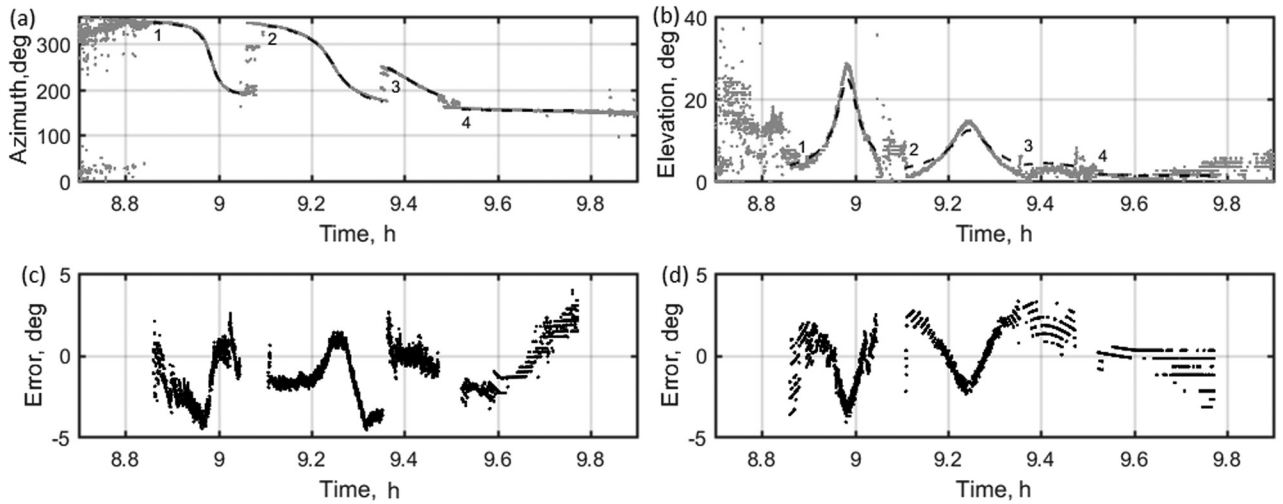

FIG. 4. (a) Azimuth estimates (gray dots) and GPS-based azimuths of vessels 1–4 (dashed lines). (b) Elevation estimates (gray dots) and GPS-based elevations of vessels 1–4 (dashed lines). (c) Azimuth estimation errors. (d) Elevation estimation errors.

$var\{b_\theta\} \gg var\{\varepsilon_\theta\}$. In fact, large deviations in azimuth and elevation estimates occur due to the presence of large errors in TDOA estimates, such that the TDOA estimates measured in *in situ* test can be modeled as

$$\hat{\tau}_{i,j} = \tau_{i,j}(\boldsymbol{\theta}) + b_{i,j} + \varepsilon_{i,j}, \tag{26}$$

where $b_{i,j}$ and $\varepsilon_{i,j}$ are random values with long and short correlation intervals, respectively; and $var\{b_{i,j}\} \gg var\{\varepsilon_{i,j}\}$.

Taking into account (25), (26), in this work we evaluated the empirical standard deviations of (1) small TDOA errors, $\varepsilon_{i,j}$; (2) large errors, b_θ; and (3) small errors, ε_θ, of azimuth and elevation estimates as functions of range. For this purpose, we used non-overlapping short-time estimates of the corresponding parameters computed using 10 s data segments. Since TDOA, azimuth, and elevation angles were measured every 0.5 s, a total of 20 independent estimates of $\hat{\tau}_{i,j}$, $\hat{\alpha}$ and $\hat{\beta}$ were computed for each data segment. We assumed that changes of large errors over a 10 s interval are negligibly small.

Let $T(m, r_k)$ be the time interval during which the mth vessel stays at the range $r \in r_k \pm \Delta$ from the compact array. Here r_k belongs to the grid of ranges $r_k \in \{100, 300, 500, \ldots, 6000\}\, m$ and $\Delta = 100\, m$. The time interval $T(m, r_k)$ consists of $P(m, r_k) = T(m, r_k)/10$ short-time intervals 10 s length each. The large error of the parameter $\theta \in \{\alpha, \beta\}$ for the pth short-time interval of the mth vessel staying at the range $r \in r_k \pm \Delta$ was computed as a median value of errors observed on this interval:

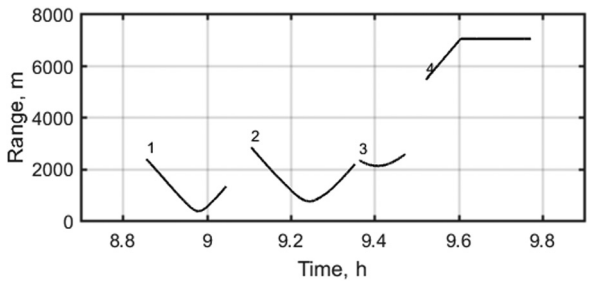

FIG. 5. GPS-based ranges of vessels 1–4.

$$\bar{b}_\theta(p) = \text{median}\{\delta_\theta(1),\, \delta_\theta(2), \ldots, \delta_\theta(20)\}, \tag{27}$$

where $\delta_\theta(k)$ is the kth estimation error (25) observed on the pth short-time interval. The empirical short-time variance of small TDOA estimation errors observed on the pth short interval was computed as

$$\hat{\sigma}^2(p) = (LK)^{-1} \sum_{l=1}^{L} \sum_{i} \sum_{j} (\hat{\tau}_{i,j}(l) - \bar{\tau}_{i,j}(p))^2, \quad i,j = 1 \ldots N,\ i < j, \tag{28}$$

where $\bar{\tau}_{i,j}(p)$ is the large TDOA error (27); L ($L = 20$) is the number of measurements per short-time interval; and $K = [N(N-1)]/2 = 6$ is the number of independent measurements of TDOAs. Correspondingly, empirical short-time variance of the small azimuth and elevation errors for the pth short-time interval was computed as

$$\hat{\sigma}_\theta^2(p) = (L)^{-1} \sum_{l=1}^{L} (\hat{\theta}(l) - \bar{b}_\theta(p))^2, \quad \theta \in \{\alpha, \beta\}. \tag{29}$$

The empirical STD of large azimuth and elevation error for the mth vessel staying at the range $r \in r_k \pm \Delta$ was computed as

$$\text{STD}_b(m, r_k) = \sqrt{(P(m, r_k))^{-1} \sum_{p=1}^{P(m,r_k)} (\bar{b}_\theta(p))^2}, \tag{30}$$

and the empirical STD of small TDOA, azimuth, and elevation errors was

$$\text{STD}_\tau(m, r_k) = (P(m, r_k))^{-1} \sum_{p=1}^{P(m,r_k)} \hat{\sigma}(p). \tag{31a}$$

$$\text{STD}_\theta(m, r_k) = (P(m, r_k))^{-1} \sum_{p=1}^{P(m,r_i)} \hat{\sigma}_\theta(p). \tag{31b}$$

For any range r_k, the median value of the empirical STD of large errors (30) and small errors (31) was evaluated as

$$\mathrm{STD}_x^{\mathrm{med}}(r_k) = \mathrm{median}\{\mathrm{STD}_x(1, r_k), \mathrm{STD}_x(2, r_k), \ldots, \mathrm{STD}_x(M_k, r_k)\}, \quad (32)$$

where M_k is the number of vessels that had the range $r \in r_k \pm \Delta$. In (32) the following notations are used: $x = \tau$ for small TDOA errors (31a), $x = \alpha$ and $x = \beta$ for small azimuth and elevation errors (31b), and $x = b$ for large azimuth and elevation errors (30), respectively. The ranges for which four or more vessels were observed, $M_k \geq 4$, were considered in the tests. The plots of median STD of large and small errors as functions of range (32) are represented in Figs. 6 and 7.

VI. DISCUSSION

The results of the statistical simulations (see Figs. 2 and 3) confirm the theory that if TDOA estimation errors are Gaussian variables, the azimuth and elevation estimation error provided by the ML locator is close to the CRB. Statistical simulations also confirm the expected result that the azimuth estimation accuracy depends on the source range relative to the array and decreases as the range increases (see Fig. 2). The other expected result is that the azimuth and elevation estimation accuracy depends on the STD of TDOA estimates, σ. The RMSE (24) decreases as the STD of TDOA estimates increases (see Fig. 3). The new and important result here is that in all simulations, the 2D ML estimator (10), the 1D ML estimator (11), and SF algorithm (17) provided basically the same accuracy.

It is important to note that both CRB and empirical RMSE depend on the number of TDOA estimates used to compute azimuths and elevations. We tested the scenario of a full set of $[N(N-1)]/2 = 6$ independent TDOA estimates used to compute azimuths and elevations. In the case of using a reduced number of $N-1$ TDOA estimates as in Refs. 2–7, 10, and 11, both the CRB and RMSE values were higher in $N/2 = 2$ times as compared to the values shown in Figs. 2 and 3.

The results of *in situ* tests show that statistical properties of both azimuth and elevation estimates obtained in real world scenarios can significantly differ from those observed in simulations based on i.i.d. Gaussian TDOA estimation errors. As Fig. 4 indicates, azimuth and elevation errors can be represented as a sum of two components with different

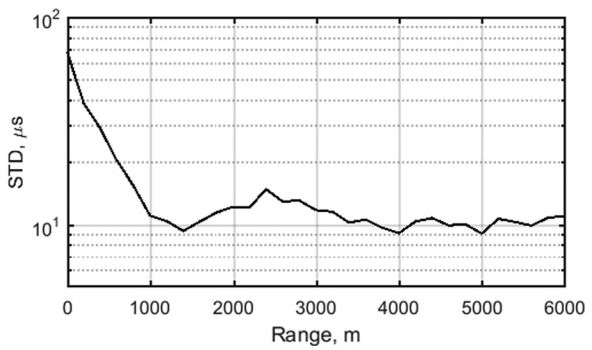

FIG. 6. STD of small TDOA errors as a function of range.

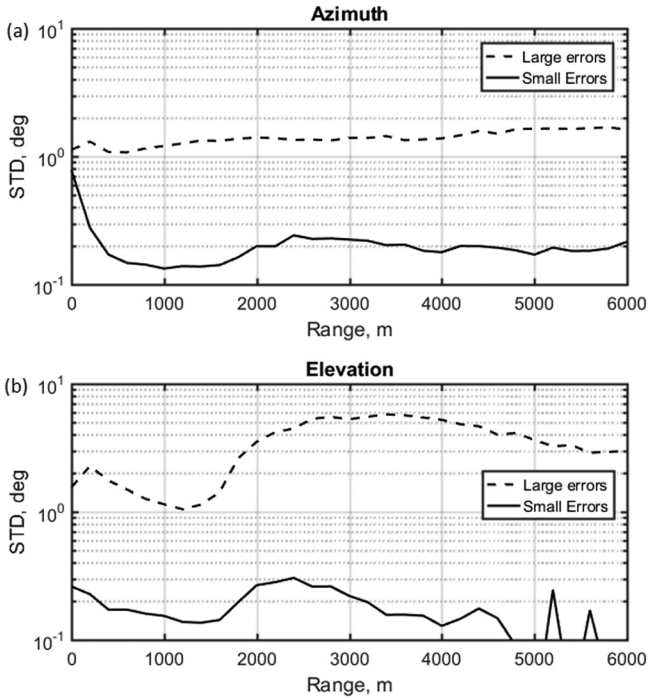

FIG. 7. STD of large and small errors as a function of range: (a) azimuth; and (b) elevation.

statistical properties. The first component, referred to as large errors, is characterized by slow changes and high variance. The second component, referred to as small errors, is similar to errors occurring due to the presence of i.i.d. Gaussian errors in TDOA estimates.

The presence of large errors in azimuth and elevation estimates can be explained by the effects of sound propagation in the water, such as refraction, surface and bottom reflections, tides, etc. The sound propagation effects affect the TDOA estimation errors such that the standard Gaussian model (7) becomes inaccurate. A more realistic model, such as that of (26), should include the presence of random components with long and short correlation interval and different variances. Studying the influence of sound propagation in the water on the accuracy of direction finding algorithms was outside the scope of this work. We restricted our efforts by demonstrating the example of using the azimuth and elevation estimation algorithms in some practical applications, such that only the standard deviations of large and small errors as functions of range were computed in this work.

The observed median value of STD of small TDOA errors was around 10 μs (see Fig. 6), and the median STD of small errors was around 0.2° for both azimuth and elevation estimates (see Fig. 7). These values are close to the theoretical CRB (23) and the empirical STD obtained in simulations (see Fig. 3). *In situ* tests also demonstrated that large errors were observed at all tested ranges and for all azimuths. No significant differences were found between the results obtained using the data collected in winter (February 21–22, 2016) and summer (August 18–23, 2016). The STD of large errors was approximately ten times higher than that of small errors (see Fig. 7).

An important result of this study is that both ML estimators (10), (11) and SF algorithms based on far field approximation of TDOAs provided very similar results. It means that the computationally efficient SF algorithm (17) can be used in many applications without loss of the estimation accuracy. However, in contrast to the unrestricted SF estimates (17), the ML estimates (10) and (11) were always found within a certain interval of azimuths and elevations. This fact is important when applying the direction finding algorithms in tracking systems where prior information about the azimuths and elevation angles of a source are available. In these systems, the grid search based algorithms can provide acceptable computational efficiency and exclude the presence of outliers.

For future research, it would be interesting to also evaluate the maximum likelihood and search free estimators with sounds produced by marine mammals. For this purpose, the accurate position of these sources would need to be known.

VII. CONCLUSIONS

The closed-form representations for the maximum likelihood and search-free TDOA-based azimuth and elevation estimation algorithms applicable for the compact arrays of hydrophones were provided. Simulations and *in situ* tests confirmed that estimation accuracy depends on the TDOA estimation error. If the source is located in the far field, all estimators provide accuracy close to the CRB.

The actual azimuth and elevation estimation accuracy achievable using compact arrays strongly depends on effects of sound propagation in water, the array deployment, and other unpredictable factors. In real conditions, the main cause of azimuth and elevation errors is the sound propagation effects resulting in large and slowly changing errors. Investigating the specific influences of these factors were outside of the scope of this work.

Simulations and *in situ* tests demonstrated that compact arrays are powerful tools for solving various practical problems arising in long-term passive acoustic monitoring, such as detecting sounds, estimating and tracking the position of sources, target motion analysis, and more.

ACKNOWLEDGMENTS

The authors thank the JASCO field team for deploying the compact array and K. Hiltz for help editing the draft version of the manuscript. The authors also thank the anonymous reviewers for their comments that helped to improve the quality of this manuscript.

[1]W. R. Hahn, "Optimum signal processing for passive sonar range and bearing estimation," J. Acoust. Soc. Am. **58**(1), 201–207 (1975).
[2]W. M. X. Zimmer, *Passive Acoustic Monitoring of Cetaceans* (Cambridge University Press, Cambridge, UK, 2011), pp. 212–215.
[3]W. M. X. Zimmer, "Range estimation of cetaceans with compact volumetric arrays," J. Acoust. Soc. Am. **134**(3), 2610–2618 (2013).
[4]R. Hirotsu, M. Yanagisawa, T. Ura, M. Sakata, H. Sugimatsu, J. Kojima, and R. Bahl, "Localization of sperm whales in a group using clicks received at two separated short baseline arrays," J. Acoust. Soc. Am. **127**(1), 133–147 (2010).
[5]S. M. Wiggins, M. A. McDonald, and J. A. Hildebrand, "Beaked whale and dolphin tracking using a multichannel autonomous acoustic recorder," J. Acoust. Soc. Am. **131**(1), 156–163 (2012).
[6]S. M. Wiggins, K. E. Frasier, E. E. Henderson, and J. A. Hildebrand, "Tracking dolphin whistles using an autonomous acoustic recorder array," J. Acoust. Soc. Am. **133**(6), 3813–3818 (2013).
[7]M. Gassmann, E. E. Henderson, S. M. Wiggins, M. Roch, and J. A. Hildebrand, "Offshore killer whale tracking using multiple hydrophone arrays," J. Acoust. Soc. Am. **134**(5), 3513–3521 (2013).
[8]M. Gassmann, S. M. Wiggins, and J. A. Hildebrand, "Three-dimensional tracking of Cuvier's beaked whales' echolocation sounds using nested hydrophone arrays," J. Acoust. Soc. Am. **138**(4), 2483–2494 (2015).
[9]D. Mathias, A. M. Thode, J. Straley, and R. D. Andrews, "Acoustic tracking of sperm whales in the Gulf of Alaska using a two-element vertical array and tags," J. Acoust. Soc. Am. **134**(3), 2446–2461 (2013).
[10]A. Tesei, S. Fioravanti, V. Grandi, P. Guerrini, and A. Maguer, "Localization of small surface vessels through acoustic data fusion of two tetrahedral arrays of hydrophones," in *Proceedings of the 11th European Conference on Underwater Acoustics* (2012), pp. 1–12.
[11]K. W. Chung, A. Sutin, A. Sedunov, and M. Bruno, "DEMON acoustic ship signature measurements in an Urban harbor," Adv. Acoust. Vib. **2011**, 952798 (2011).
[12]C. Hillis, X. Mouy, I. Urazghildiiev, and T. Dakin, "Autonomous multichannel acoustic recorders on the VENUS ocean observatory," in *Oceans'2014*, St. John's, Canada (2014).
[13]V. H. McDonald and P. M. Schultheiss, "Optimum passive bearing estimation," J. Acoust. Soc. Am. **45**(1), 294 (1969).
[14]U. Datta, R. Otnes, and C. Lucas, "Bearing estimation using small tetrahedral passive hydrophone array," in *Oceans'2010* (September 20–23, 2010).
[15]J. Gebbie, M. Siderius, P. L. Nielsen, and J. Miller, "Passive localization of noise-producing targets using a compact volumetric array," J. Acoust. Soc. Am. **136**(1), 80–89 (2014).
[16]E. M. Nosal and L. N. Frazer, "Sperm whale three-dimensional track, swim orientation, beam pattern, and click levels observed on bottom-mounted hydrophones," J. Acoust. Soc. Am. **122**(4), 1969–1978 (2007).
[17]I. R. Urazghildiiev and C. W. Clark, "Comparative analysis of localization algorithms with application to passive acoustic monitoring," J. Acoust. Soc. Am. **134**(6), 4418–4426 (2013).
[18]H. L. Van Trees, *Optimal Array Processing. Part IV of Detection, Estimation, and Modulation Theory* (Wiley, New York, 2002), pp. 938–984.
[19]S. M. Kay, *Fundamentals of Statistical Signal Processing. Estimation Theory* (Prentice Hall, Englewood Cliffs, NJ, 1993).
[20]J. Weng and K. Y. Guentchev, "Three-dimensional sound localization from a compact non-coplanar array of microphones using tree-based learning," J. Acoust. Soc. Am. **110**(1), 310–323 (2001).
[21]D. J. Mennill, M. Battison, R. R. Wilson, J. R. Foote, and S. M. Doucet, "Field test of an affordable, portable, wireless microphone array for spatial monitoring of animal ecology and behavior," Meth. Ecol. Evol. **3**, 704–712 (2012).
[22]G. H. Goldman, "Tracking unmanned aerial vehicles using a tetrahedral microphone array," J. Acoust. Soc. Am. **136**(4), 2213 (2014).